Supporting Information

Quantum Mechanical/Molecular Mechanical Study on the Enantioselectivity of the Enzymatic Baeyer-Villiger Reaction of 4-Hydroxycyclohexanone

Iakov Polyak[†], *Manfred T. Reetz*[†,‡], *and Walter Thiel**[,†]

[†]Max-Planck-Institut für Kohlenforschung, Kaiser-Wilhelm-Platz 1, D-45470 Mülheim an der Ruhr, Germany; [‡]Fachbereich Chemie, Philipps-Universität Marburg, Hans-Meerwein-Straße, D-35032 Marburg, Germany

Contents

Energy diagrams

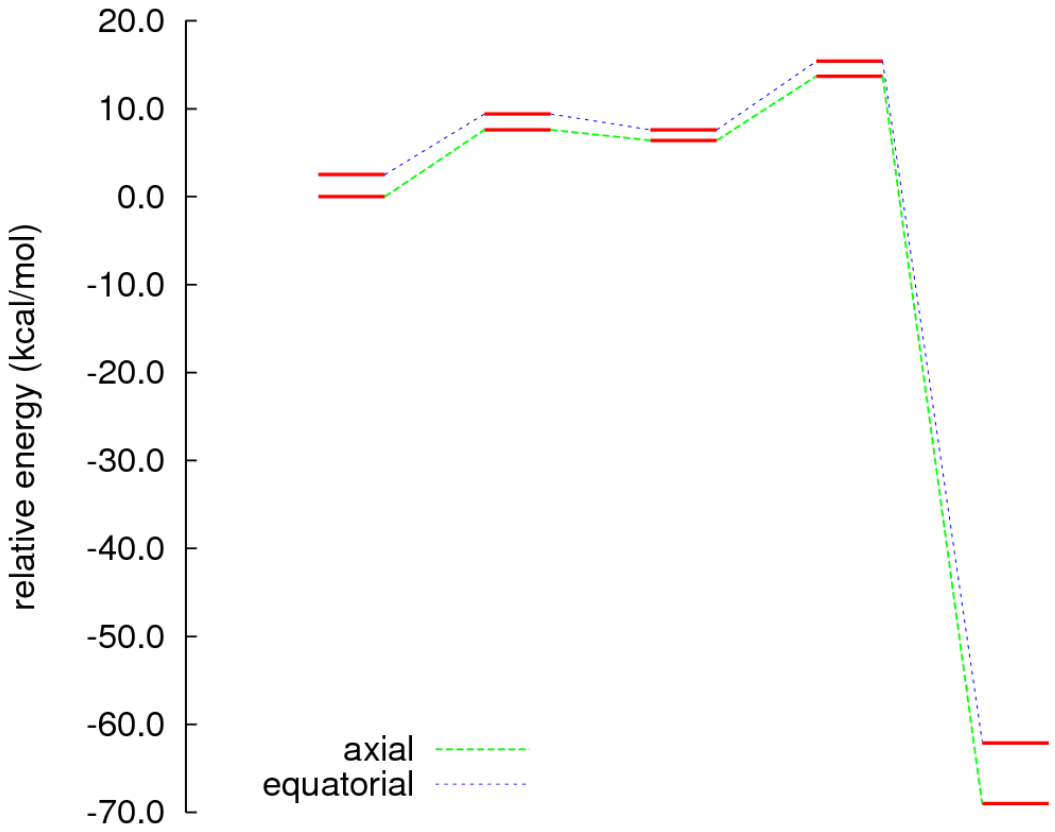

Figure S1. QM(B3LYP/TZVP)/CHARMM energy profiles for the WT CHMO (*Rhodococcus*) with the hydroxyl group of **1** in equatorial and axial position. From left to right, the energy levels correspond to the reactant complex, the transition state for the addition step (TS1), the Criegee intermediate, the transition state for the migration step (TS2), and the product complex. The energy profiles have been computed using the small QM region 1(see below). For energy values, see Table S1.

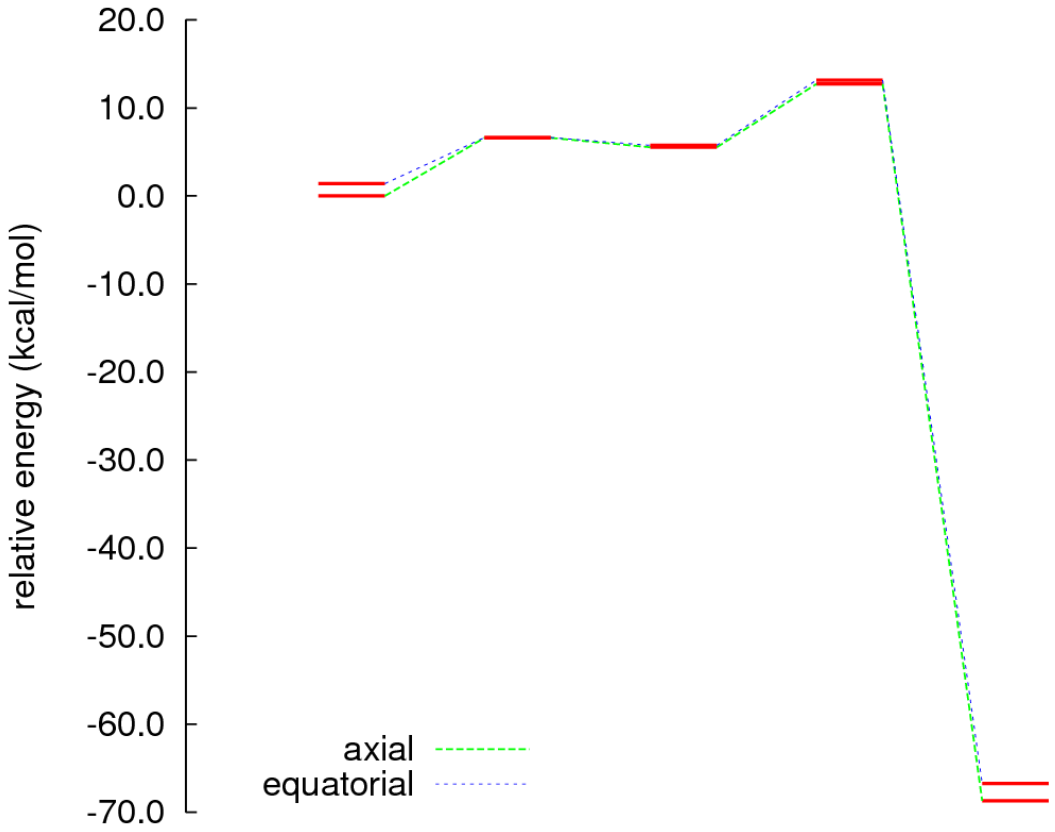

Figure S2. QM(B3LYP/TZVP)/CHARMM energy profiles for the Phe434Ser mutant of CHMO (*Rhodococcus*) with the hydroxyl group of **1** in equatorial and axial position. From left to right, the energy levels correspond to the reactant complex, the transition state for the addition step (TS1), the Criegee intermediate, the transition state for the migration step (TS2), and the product complex. The energy profiles have been computed using the small QM region 1 (see below). For energy values, see Table S2.

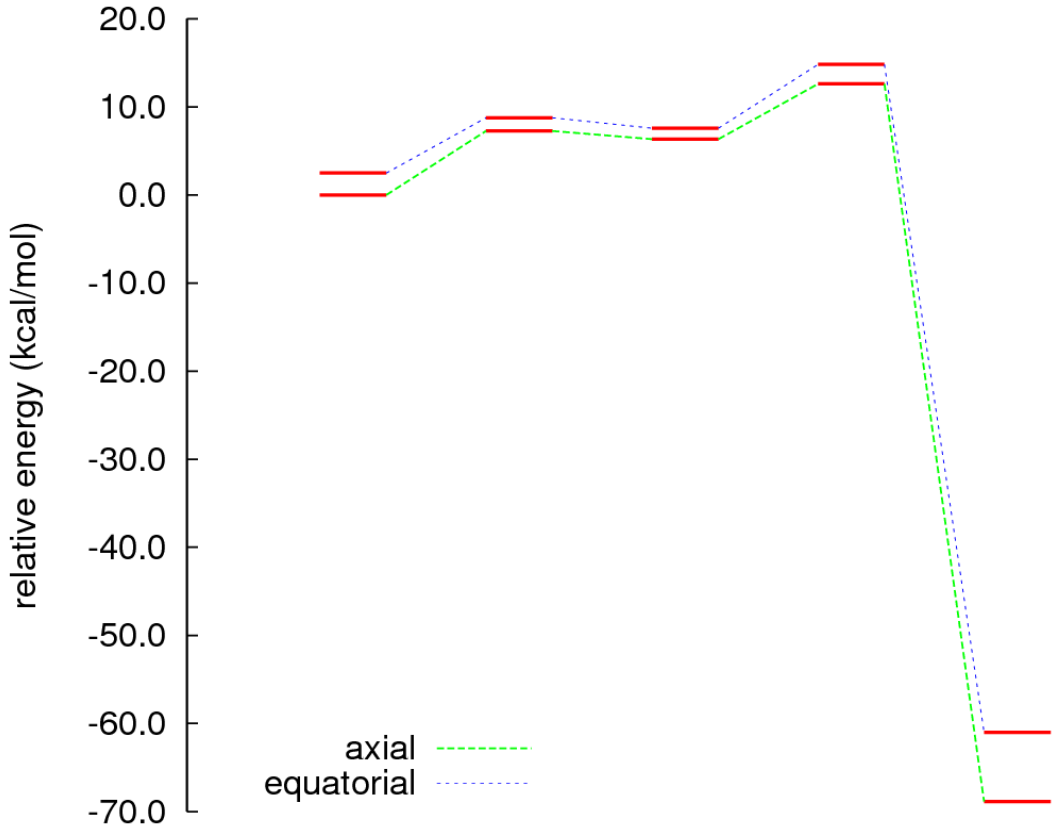

Figure S3. QM(B3LYP/TZVP)/CHARMM energy profiles for the Phe434Ile mutant of CHMO (*Rhodococcus*) with the hydroxyl group of **1** in equatorial and axial position. From left to right, the energy levels correspond to the reactant complex, the transition state for the addition step (TS1), the Criegee intermediate, the transition state for the migration step (TS2), and the product complex. The energy profiles have been computed using the small QM region 1 (see below). For energy values, see Table S3.

	Reactant	TS1 scan	Intermediate	TS2	Product
Equatorial	2.5	9.4	7.6	15.4	-62.1
Axial	0.0	7.6	6.4	13.7	-69.0

Table S1. Calculated QM(B3LYP/TZVP)/CHARMM energies (in kcal/mol) for stationary points along the reaction profile for the WT CHMO (*Rhodococcus*) with the hydroxyl group of **1** in equatorial and axial position. The energy profiles have been computed using the small QM region 1 (see below). Energies are given relative to the reactant complex with axial configuration.

	Reactant	TS1 scan	Intermediate	TS2	Product
Equatorial	1.4	6.6	5.7	13.2	-66.7
Axial	0.0	6.6	5.5	12.7	-68.7

Table S2. Calculated QM(B3LYP/TZVP)/CHARMM energies (in kcal/mol) for stationary points along the reaction profile for the Phe434Ser mutant of CHMO (*Rhodococcus*) with the hydroxyl group of **1** in equatorial and axial position. The energy profiles have been computed using the small QM region 1 (see below). Energies are given relative to the reactant complex with axial configuration.

	Reactant	TS1 scan	Intermediate	TS2	Product
Equatorial	2.5	8.8	7.6	14.8	-61.0
Axial	0.0	7.3	6.3	12.6	-68.9

Table S3. Calculated QM(B3LYP/TZVP)/CHARMM energies (in kcal/mol) for stationary points along the reaction profile for the Phe434Ile mutant of CHMO (*Rhodococcus*) with the hydroxyl group of **1** in equatorial and axial position. The energy profiles have been computed using the small QM region 1 (see below). Energies are given relative to the reactant complex with axial configuration.

Please note:

The transition states TS2 have been reoptimized at the QM(B3LYP/TZVP)/CHARMM level using the larger QM regions 2 and 3 (see below). The resulting energy differences between the TS2 structures containing the equatorial and axial substrate conformers are given in Table 1 of the main paper for the WT CHMO enzyme and the two mutants. They are considered more reliable than those derived from Tables S1-S3 because of the use of larger QM regions.

QM regions

WT CHMO

QM region 1 : Isoalloxazine ring of the peroxyflavin, ligand (**1**), the side chain of Arg329, the nicotineamide ring and the adjacent ribose of $NADP^+$ cofactor (97 atoms).

QM region 2 : Isoalloxazine ring of the peroxyflavin, ligand (**1**), the side chain of Arg329, the nicotineamide ring and the adjacent ribose of $NADP^+$ cofactor; the carbonyl group of Phe434; the full backbone of Thr435; the amino group and the α-CH group of Asn436 (109 atoms).

QM region 3 : Isoalloxazine ring of the peroxyflavin, ligand (**1**), the side chain of Arg329, the nicotineamide ring and the adjacent ribose of $NADP^+$ cofactor; the carbonyl group, the α-CH group, and the side-chain of Phe434; the full backbone of Thr435; the amino group and the α-CH group of Asn436 (127 atoms).

Phe434Ser mutant of CHMO

QM region 1 : Isoalloxazine ring of the peroxyflavin, ligand (**1**), the side chain of Arg329, the nicotineamide ring and the adjacent ribose of $NADP^+$ cofactor (97 atoms).

QM region 2 : Isoalloxazine ring of the peroxyflavin, ligand (**1**), the side chain of Arg329, the nicotineamide ring and the adjacent ribose of $NADP^+$ cofactor; the side chain of Ser434; the carbonyl group of Thr435; the amino group and the α-CH group of Asn436 (108 atoms).

Phe434Ile mutant of CHMO

QM region 1 : Isoalloxazine ring of the peroxyflavin, ligand (**1**), the side chain of Arg329, the nicotineamide ring and the adjacent ribose of $NADP^+$ cofactor (97 atoms).

QM region 2 : Isoalloxazine ring of the peroxyflavin, ligand (**1**), the side chain of Arg329, the nicotineamide ring and the adjacent ribose of $NADP^+$ cofactor; the carbonyl group of Ile434; the full backbone of Thr435; the amino group and the α-CH group of Asn436 (109 atoms).

Ligand hydroxyl group rotation in the Criegee intermediate of the WT CHMO.

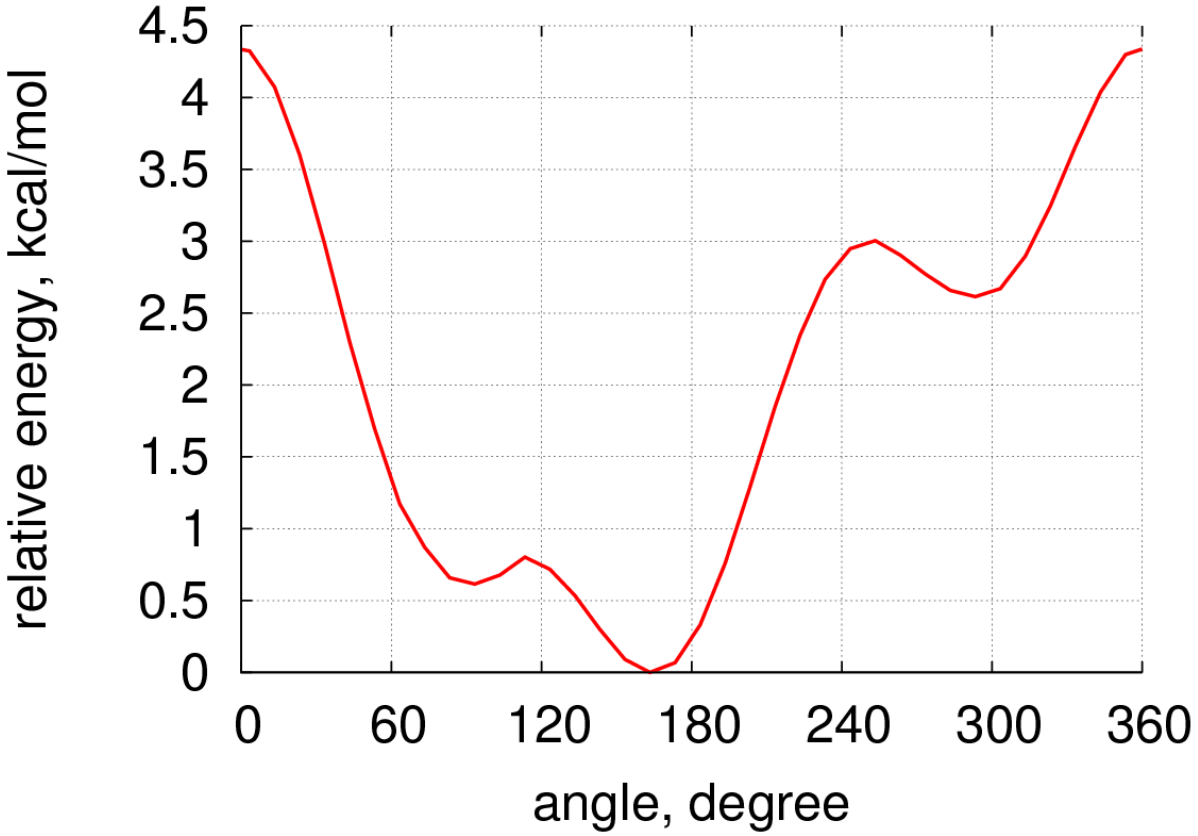

Figure S4. Energy profile for rotation of the equatorial hydroxyl group of the ligand (**1**) in the Criegee intermediate of the WT CHMO (*Rhodococcus*) from QM/MM geometry optimizations using the small QM region 1. At the energy minimum, the hydroxyl group is oriented towards the benzene ring of the Phe434 side chain, creating a weak π-hydroxyl H-bond. This orientation was adopted in the computation of the energy profile of the enzymatic Baeyer-Villiger reaction.

Ser434 – ligand hydrogen bond dynamics

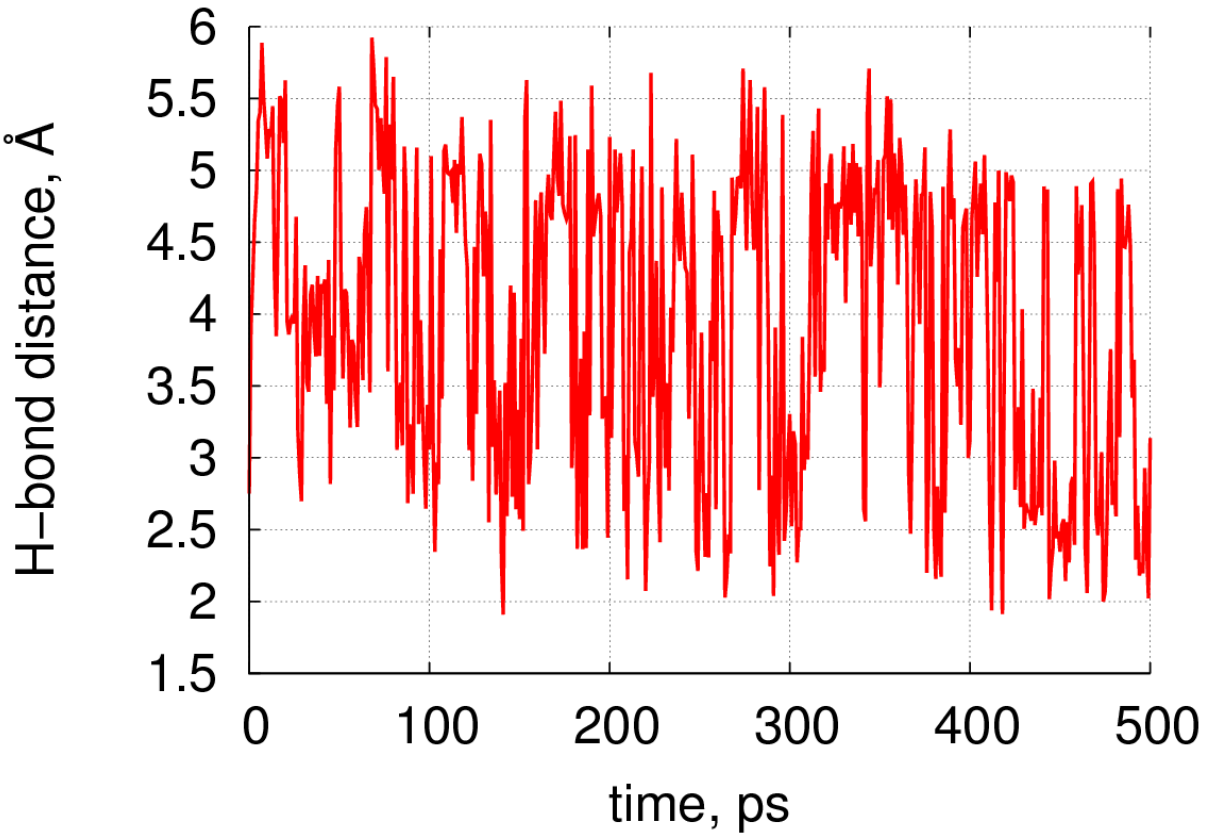

Figure S5. Changes in the H-bonding distance between the hydrogen atom of the Ser434 hydroxyl group and the oxygen atom of the equatorial ligand hydroxyl group during the 500ps classical MD sampling run.

Evaluation of the *ee* value (enantiomeric excess)

We evaluate the *ee* value from the following formula:

$$ee = \frac{\exp(-\frac{\Delta E^{TS}}{RT}) - 1}{\exp\left(-\frac{\Delta E^{TS}}{RT}\right) + 1} * 100\%$$

Here, $\Delta E^{TS} = E^{TS}_{favoured} - E^{TS}_{disfavoured}$ is the difference between the QM/MM energies of the rate-determining transition states TS2 containing the equatorial and axial substrate conformers. We take the difference between the absolute TS2 energies because at equilibrium the initial reference state is the same for both conformers, namely the lowest-energy reactants at infinite separation (enzyme and substrate). In this manner we also account for the energy difference between the two isolated conformers.

Strictly speaking, we would need to evaluate the *ee* value from differences in free energies (ΔG) rather than energies (ΔE). In the above formula, we approximate the free energies of the transition states by their potential energies, assuming that the differences in the corresponding zero-point vibrational energies and thermal corrections are negligibly small.

Conversely, we can determine the energy difference associated with the experimental *ee* value (given as a decimal number in the range 0-1 rather than in percent):

$$\Delta E^{TS} = RT \ln\left(\frac{1 + ee}{1 - ee}\right)$$

Complete references 12, 13b, 14 and 17 of the main paper

12. MacKerell, A. D.; Bashford, D.; Bellott, M.; Dunbrack, R. L.; Evanseck, J. D.; Field, M. J.; Fischer, S.; Gao, J.; Guo, H.; Ha, S.; Joseph-McCarthy, D.; Kuchnir, L.; Kuczera, K.; Lau, F. T. K.; Mattos, C.; Michnick, S.; Ngo, T.; Nguyen, D. T.; Prodhom, B.; Reiher, W. E.; Roux, B.; Schlenkrich, M.; Smith, J. C.; Stote, R.; Straub, J.; Watanabe, M.; Wiorkiewicz-Kuczera, J.; Yin, D.; Karplus, M., All-atom empirical potential for molecular modeling and dynamics studies of proteins. *J. Phys. Chem. B* **1998,** *102* (18), 3586-3616.

13. (b) Brooks, B. R.; Brooks, C. L., III; Mackerell, A. D., Jr.; Nilsson, L.; Petrella, R. J.; Roux, B.; Won, Y.; Archontis, G.; Bartels, C.; Boresch, S.; Caflisch, A.; Caves, L.; Cui, Q.; Dinner, A. R.; Feig, M.; Fischer, S.; Gao, J.; Hodoscek, M.; Im, W.; Kuczera, K.; Lazaridis, T.; Ma, J.; Ovchinnikov, V.; Paci, E.; Pastor, R. W.; Post, C. B.; Pu, J. Z.; Schaefer, M.; Tidor, B.; Venable, R. M.; Woodcock, H. L.; Wu, X.; Yang, W.; York, D. M.; Karplus, M., CHARMM: The Biomolecular Simulation Program. *J. Comput. Chem.* **2009,** *30* (10), 1545-1614.

14. Vanommeslaeghe, K.; Hatcher, E.; Acharya, C.; Kundu, S.; Zhong, S.; Shim, J.; Darian, E.; Guvench, O.; Lopes, P.; Vorobyov, I.; MacKerell, A. D., CHARMM General Force Field: A Force Field for Drug-Like Molecules Compatible with the CHARMM All-Atom Additive Biological Force Fields. *J. Comput. Chem.* **2010,** *31* (4), 671-690.

17. Sherwood, P.; de Vries, A. H.; Guest, M. F.; Schreckenbach, G.; Catlow, C. R. A.; French, S. A.; Sokol, A. A.; Bromley, S. T.; Thiel, W.; Turner, A. J.; Billeter, S.; Terstegen, F.; Thiel, S.; Kendrick, J.; Rogers, S. C.; Casci, J.; Watson, M.; King, F.; Karlsen, E.; Sjovoll, M.; Fahmi, A.; Schäfer, A.; Lennartz, C., QUASI: A general purpose implementation of the QM/MM approach and its application to problems in catalysis. *Theochem* **2003,** *632*, 1-28.